

# Quasi-static remanence as a generic-feature of spin-canting in Dzyaloshinskii-Moriya Interaction driven canted-antiferromagnets.

Namrata Pattanayak<sup>1,2</sup>, Arun Kumar<sup>1</sup>, A.K Nigam<sup>3</sup>, Vladimir Pomjakushin<sup>4</sup>, Sunil Nair<sup>1</sup>, Ashna Bajpai<sup>1</sup>

<sup>1</sup>*Department of Physics, Indian Institute of Science Education and Research, Pune, India*

<sup>2</sup>*Department of Physics, NIST, Berhampur, Odisha, 761008, India*

<sup>3</sup>*Tata Institute of Fundamental research, India and*

<sup>4</sup>*Laboratory for Neutron Scattering and Imaging, Paul Scherrer Institut, Villigen, CH-5232, Switzerland*

(\*ashna@iiserpune.ac.in)

(Dated: October 31, 2023)

We consistently observe a unique pattern in remanence in a number of canted-antiferromagnets (AFM) and piezomagnets. A part of the remanence is *quasi-static* in nature and vanishes above a critical magnetic field. Present work is devoted to exploring this *quasi-static* remanence ( $\mu$ ) in a series of isostructural canted-AFM and piezomagnets that possess progressively increasing Néel temperature ( $T_N$ ). Comprehensive investigation of remanence as a function of *magnetic-field* and *time* in  $\text{CoCO}_3$ ,  $\text{NiCO}_3$  and  $\text{MnCO}_3$  reveals that the magnitude of  $\mu$  increases with decreasing  $T_N$ , but the stability with time is higher in the samples with higher  $T_N$ . Further to this, all three carbonates exhibit a universal scaling in  $\mu$ , which relates to the concurrent phenomenon of piezomagnetism. Overall, these data not only establish that the observation of *quasi-static* remanence with *counter-intuitive* magnetic-field dependence can serve as a foot-print for spin-canted systems, but also confirms that simple remanence measurements, using SQUID magnetometry, can provide insights about the extent of spin canting - a non trivial parameter to determine. In addition, these data suggest that the functional form of  $\mu$  with *magnetic-field* and *time* may hold key to isolate Dzyaloshinskii Moriya Interaction driven spin-canted systems from Single Ion Anisotropy driven ones. We also demonstrate the existence of  $\mu$  by tracking specific peaks in neutron diffraction data, acquired in remnant state in  $\text{CoCO}_3$ .

Canted-antiferromagnets or *weak ferromagnets* leading to exotic chiral spin structures form one of the most niche area of fundamental and applied research. [1–8]. The phenomenon of spin-canting is understood to arise from two primary mechanisms, one of which is the celebrated Dzyaloshinski -Moriya Interaction (DMI) and the other relates to Single Ion Anisotropy (SIA)[9, 10]. Hematite ( $\alpha\text{-Fe}_2\text{O}_3$ ) along with a series of isostructural carbonates ( $\text{MnCO}_3$ ,  $\text{NiCO}_3$  &  $\text{CoCO}_3$ ) and rutile fluorides ( $\text{NiF}_2$  and  $\text{CoF}_2$ ) constitute the canonical examples of DMI and SIA driven canted-AFM respectively[9, 10]. It is to be noted that spin canting in  $\text{CoCO}_3$  is understood to have contributions from both DMI as well as SIA [11]. This sets  $\text{CoCO}_3$  apart from primarily DMI-driven canted AFM ( $\alpha\text{-Fe}_2\text{O}_3$ ,  $\text{MnCO}_3$  &  $\text{NiCO}_3$ ) and also from primarily SIA-driven canted AFM ( $\text{NiF}_2$  and  $\text{CoF}_2$ ). All these canted AFMs, driven by either DMI or SIA are also known to be symmetry allowed piezomagnets (PzMs)[9, 10].

Notably, some of these symmetry allowed canted-AFM & PzMs have shown some unique features in *remanence* measurements. These measurements conducted on single crystal, mesoscopic & nano-scale Hematite crystallites [12, 13], hematite inside carbon nanotubes [14] as well as on the mesoscopic crystallites of  $\text{MnCO}_3$  [13] bring out two unique features. First is that there exist two distinct time scales related to the magnetization dynamics, one of which is *ultra-slow* in nature. This ultra slow magnetization relaxation results in the observation of *quasi static remanence*, which is referred to as  $\mu$  throughout the text. Second feature is that the  $\mu$  shows a counter-intuitive magnetic field dependence. These specific traits set remanence in *canted-AFM* apart from the one observed in a routine ferromagnetic (FM), antiferromagnetic or a spin glass phase. The magnitude of this  $\mu$  is tunable with nanoscaling [12, 13] as well as with interface effects[14] in

above mentioned systems -which are symmetry allowed DMI driven canted AFMs. However, Ultra thin films of  $\text{Cr}_2\text{O}_3$  [15], composites of  $\text{CrO}_2/\text{Cr}_2\text{O}_3$  [16] and encapsulation of  $\text{Cr}_2\text{O}_3$  inside carbon nanotubes [17] also exhibited very similar traits in  $\mu$ , implying novel strain & interface effects leading to spin-canting and PzM.

In the present work, we have extended our investigation pertaining to  $\mu$  in a series of canonical spin-canted systems, that possess systematically varying  $T_N$ . It is to be noted that larger spin canting angle is expected in samples with lower  $T_N$ . Also, the spin canting angle is a non trivial parameter to measure and it takes painstaking efforts to estimate the direction or the magnitude of spin canting[11, 18, 19]. In this work, our endeavor is to establish the presence of  $\mu$  as a generic feature in spin-canted AFM and PzM and explore the correlations between this unique  $\mu$  and the extent of spin-canting, which in -turn relates to  $T_N$ . In addition, we observe a universal scaling in  $\mu$  which has been earlier reported for symmetry allowed piezomagnets, or samples in which piezomagnetism emerges due to size and interface effects [15–17, 20]. Apart from remanence measurements using SQUID magnetometry, we also present a microscopic experimental evidence for existence of  $\mu$  using neutron diffraction experiments in a representative carbonate,  $\text{CoCO}_3$ .

## I. EXPERIMENTAL TECHNIQUES

The carbonates presented in this work are synthesized by the hydrothermal technique (Supp.Info: Text S1) and the phase purity is confirmed using X-ray diffraction, along with the Rietveld Profile refinement of the XRD data (Supp.Info : Figure S1). The lattice parameters determined from Rietveld

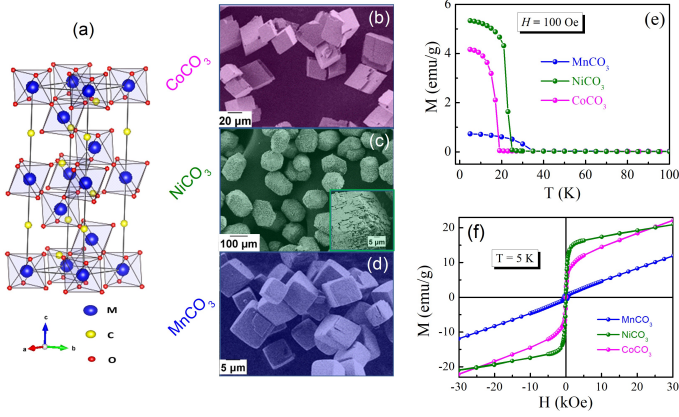


FIG. 1. (a) Schematic unit cell of isostructural carbonates with M being metal ion. (b)- (c) depict SEM images of CoCO<sub>3</sub>, NiCO<sub>3</sub> and MnCO<sub>3</sub> respectively. Samples consists of regular shaped polyhedra, with size ranging from a few tens of microns to 100 microns. (e) shows  $M$  as a function of  $T$  measured at 100 Oe & (f) shows  $M$  vs  $H$  isotherms at 5K for CoCO<sub>3</sub> (pink dots), NiCO<sub>3</sub> (green dots) and MnCO<sub>3</sub> (blue dots).

profile refinement are shown in Table 1 in Supp. Information. The schematic unit cell for the carbonates, which crystallize in rhombohedral structure is depicted in Figure 1(a) and the scanning electron micrograph (SEM) are shown in Figure 1(b)-(d). The size range of individual crystallites falling in bulk limit ensures that the remanence data presented in this work is not associated with nano-scaling, which can also lead to a slow-magnetization dynamics in routine ferromagnets [21].

The  $M$  versus  $T$  are shown in Figure 1(e) for all three carbonates. The progressively increasing  $T_N$  values are 18K, 24K and 35 K for CoCO<sub>3</sub>, NiCO<sub>3</sub> and MnCO<sub>3</sub> respectively. These values in good agreement with the previous reports [22, 23]. Figure 1(f) compares the  $MH$  isotherms at 5K for all three samples. Here the  $M$  increases with increasing  $H$  and shows a slight opening of the loop in lower magnetic fields, followed by a non-saturating behavior in higher fields. The loop opening in lower field region is also shown as Supp. Info, Figure S2. This small loop opening is a signature of weak ferromagnetism in otherwise AFMs. However, on a general note, it is rather difficult to distinguish a canted AFM from a normal AFM or soft FM, a FM/AFM interface, or a glassy system based solely on magnetization measurement. These systems can also show small opening of the loop in  $MH$  and mimic FM like behavior  $M$  vs  $H$  or  $M$  vs  $T$ . Microscopic measurements like neutron diffraction are therefore essential for firmly establishing the AFM phase. It is all the more difficult to identify and establish canting phenomenon for samples in which the *spin-canting* is arising due to size or interface effects. Our endeavor in the present work is to show that simple *remanent magnetization* measurements can better establish a canted AFM phase.

## II. RESULTS & DISCUSSION

### A. Temperature variation of Magnetization and the corresponding Remanence in NiCO<sub>3</sub>

We first define the protocol of magnetization and corresponding remanence measurements adopted in this work. As shown in Figure 2(a), the magnetization is measured while cooling the sample, which is NiCO<sub>3</sub> in this case, from above its  $T_N$ . This is regular field-cooled cycle to obtain  $M_{FC}$  vs  $T$  data, shown as black dots in Figure 2(a). After reaching 5K, the applied  $H$  is turned off and the magnetization instantaneously drops. However it arrives to a fixed value, and does not show any further decay. This is basically the *quasi-static* part of the remanence ( $\mu$ ). We note that  $M_{FC} \sim 1.14$  emu/g and the corresponding  $\mu \sim 0.98$  emu/g at 5K. Thus the magnetization drops to about 95% of its *in-field* value. It is to be emphasized that the  $\mu$  does not exhibit any further decay with time, as long as  $T$  is held at 5K. On increasing the temperature, the  $\mu$  vs  $T$  can be measured in warming cycle (green dots in Figure 2(a)). It is evident that the  $\mu$  decreases with increasing  $T$  in a fashion which is qualitatively similar to  $M_{FC}$  vs  $T$ . It vanishes in the paramagnetic region, above the  $T_N$ .

The magnitude of this  $\mu$  depends on the magnetic field applied during the cooling cycle i.e, while measuring  $M_{FC}$  vs  $T$ . For instance, when the entire protocol is repeated for a larger cooling  $H$  of 2 kOe, the magnitude of  $M$  at 5K is  $\sim 21$  emu/g and that of the corresponding  $\mu$  is vanishingly small,  $\sim 10^{-4}$  emu/g, as is evident from Figure 2(b). Thus, we observe that there is practically no  $\mu$  for NiCO<sub>3</sub> in magnetic field of 2kOe. The small negative value of  $\mu$  for H 2kOe case is an artifact of measurement. It arises from the residual negative field of the superconducting magnet of SQUID.

For all the intermediate (cooling) magnetic fields,  $M$  vs  $T$  and the corresponding  $\mu$  vs  $T$  is presented in Figure 2(c) & Figure 2(d) respectively. The  $M$  vs  $T$  and  $\mu$  vs  $T$  are plotted in separate graphs for the sake of clarity. It is to be emphasized that all the remanence data is obtained in zero  $H$ . The magnetic field specified in the Figure 2(d) refers to the magnetic field used for preparing a remanent state while recording  $M_{FC}$  vs  $T$  cycles. We note that  $\mu$  is nearly of same magnitude as the *in-field* magnetization for lower (cooling) fields. The magnitude of  $\mu$  is maximum for the (cooling) field of 100 Oe in case of NiCO<sub>3</sub>, as is evident from Figure 2(d). Also, there is no *quasi-static*  $\mu$  above a critical magnetic field, which is  $\sim 2$  kOe in case of NiCO<sub>3</sub> (Figure 2(b)). For all the intermediate magnetic fields, the *quasi-static* remanence first increases with increasing magnetic field up to a critical field. Thereafter it starts decreasing with increasing (cooling) field and eventually vanishes, as is evident from Figure 2(d).

Following similar experimental protocol for preparing a remanent state in different magnetic fields, *quasi-static* remanence has already been reported [12] for MnCO<sub>3</sub> crystallites shown in Figure 1(d). This sample also shows a peak like behavior in  $\mu$  as a function of magnetic field, before vanishing at another critical field [12].

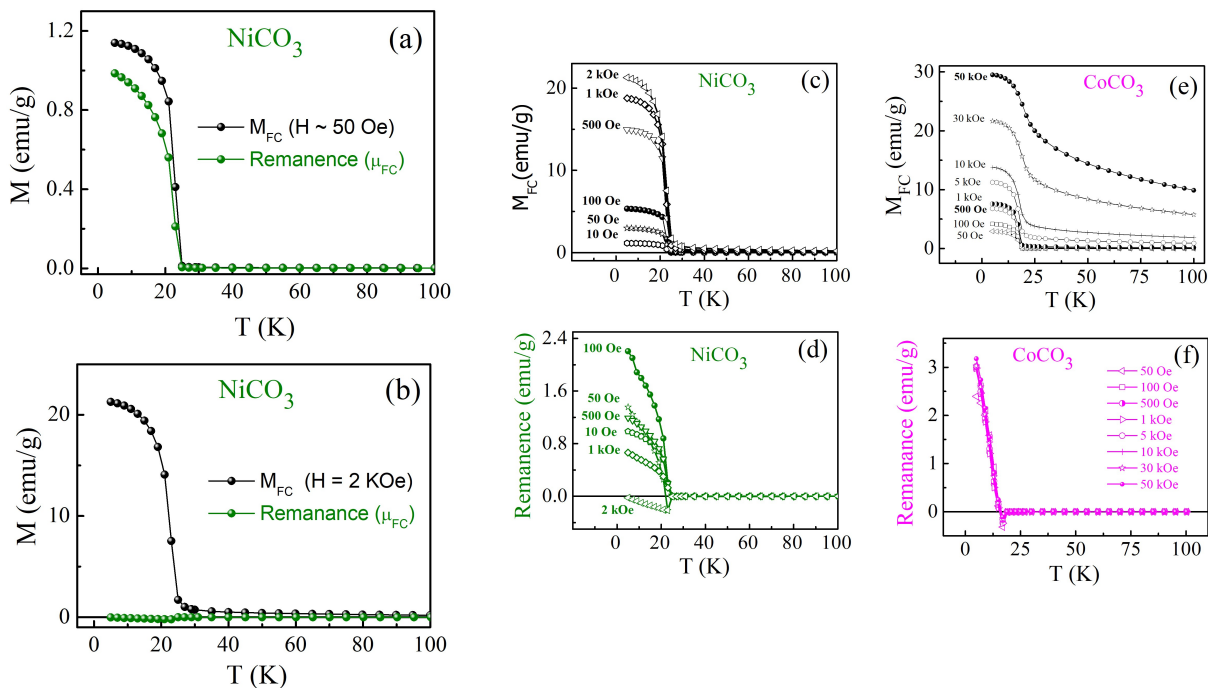


FIG. 2. (a) shows  $M$  versus  $T$  for  $\text{NiCO}_3$  in presence of 100 Oe while cooling the sample from above its  $T_N$  (black dots). At 5K the magnetic field is switched off and corresponding remanence ( $\mu$  versus  $T$ ) is measured in warming cycle (green dots). (b) shows the same for  $\text{NiCO}_3$  in  $H = 2$  kOe. (c) shows  $M$  versus  $T$  (black dots) in various  $H$  for  $\text{NiCO}_3$ . The corresponding remanence ( $\mu$ ) versus  $T$  (green dots) is plotted separately in (d). (e) & (f) show  $M$  and corresponding  $\mu$  for for  $\text{CoCO}_3$  in various (cooling) magnetic fields.

### B. Temperature variation of Magnetization and the corresponding Remanence in $\text{CoCO}_3$

The  $M$  vs  $T$  and the corresponding  $\mu$  vs  $T$  data for  $\text{CoCO}_3$ , following the similar experimental protocol as adopted for  $\text{NiCO}_3$  is presented in Figure 2(e) and Figure 2(f) respectively.  $\text{CoCO}_3$  exhibits some additional noteworthy features in  $M$  vs  $T$  cycles. For instance, the transition region is fairly broadened, especially when  $M$  is measured in higher magnetic fields. Broadening in the vicinity of magnetic transition temperature is typically attributed to short range correlations. However, in this series of carbonates, this broadening is substantial for  $\text{CoCO}_3$  as compared to the other two carbonates and this feature extends much above the  $T_N$  of  $\text{CoCO}_3$ . Another interesting observation that the  $\mu$  vs  $T$  data nearly self-scale in case of  $\text{CoCO}_3$  (Figure 2(f)). This pattern in  $\mu$  vs  $T$  of  $\text{CoCO}_3$  is strikingly different from both  $\text{NiCO}_3$ , shown in Figure 2(d) and  $\text{MnCO}_3$  [13]. Both these samples also exhibit universal scaling, albeit after the  $\mu$  at a given temperature is normalized with  $\mu$  measured at 5K. The issues of scaling will be discussed in section E. It is also interesting to note that the  $\mu$  is practically zero in the paramagnetic region for all three carbonates. We also note that the  $\mu$  vanishes in the vicinity of  $T_N$  for each compound as is evident from Figure 2 for  $\text{NiCO}_3$  and  $\text{CoCO}_3$ . Qualitatively similar data for  $\text{MnCO}_3$  is reported in reference [13]. Thus we note that  $\mu$  vs  $T$ , especially in lower  $H$ , clearly marks the intrinsic AFM transition, better than the corresponding  $M$  vs  $T$  data in all three carbonates. In addition  $\mu$  vs  $T$  measured at different  $H$  also reveal that  $\mu$  shows a

peak like behavior and vanishes above a critical field for both  $\text{MnCO}_3$  and  $\text{NiCO}_3$ . This unique pattern of remanence as a function of magnetic field sets apart canted-AFM from other magnets, as shown in the next subsection.

### C. Counter-intuitive magnetic field dependence of quasi static remanence

Our core observation here is the counter-intuitive  $H$  dependence of  $\mu$  in canted AFM, which is not reflected in the routine *in-field* measurements [12, 13, 16, 17]. To highlight this, we plot both  $M$  vs  $H$  in conjuncture with  $\mu$  vs  $H$  for all three carbonates at a fixed temperature of 5K. Here  $M$  increases with increasing magnetic field and hence the field dependence of  $M$  is regular for all three carbonates (black dots -right axis in Figure 3). The corresponding  $\mu$  (at 5K) shows an anomalous  $H$  dependence for  $\text{MnCO}_3$  (blue dots- left axis) and  $\text{NiCO}_3$  (green dots -left axis). In both cases, the magnitude of *quasi-static* remanence first increases with increasing  $H$ , followed by a drop. The remanence eventually vanishes at some  $H$ , depending on the sample. In case of  $\text{NiCO}_3$  the critical magnetic field, at which the magnitude of  $\mu$  is highest is 100 Oe, as is evident from Figure 3(b). Another critical magnetic field at which the remanence vanishes is about 2kOe for  $\text{NiCO}_3$ , as shown in Figure 3(b). These critical fields are 500 Oe and 30 kOe respectively for  $\text{MnCO}_3$ , as shown in Figure 3(c).  $\text{CoCO}_3$  also shows a tendency to peak like behavior, followed by a increases with increasing (cooling) magnetic field. It is to be

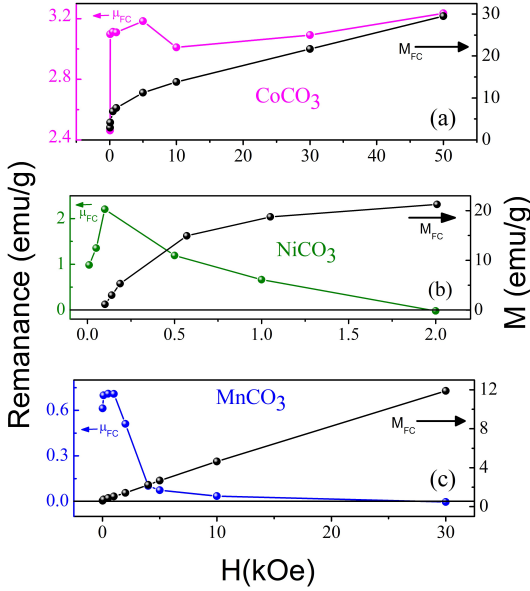


FIG. 3. (a)-(c) show field dependence of remanence ( $\mu$  vs  $H$ ) for all three carbonates in conjunction with the corresponding  $M$  vs  $H$  (black dots) at a fixed temperature of 5K. While  $M$  increases with increasing  $H$ , the corresponding remanence exhibits a peak like behaviour for  $MnCO_3$  as well as  $NiCO_3$ . In case of  $CoCO_3$ , which is understood to have contributions from SIA apart from DMI in spin-canting, a tendency of peak-like behaviors is followed by a rise in remanence upon increasing  $H$ .

noted that in case of  $CoCO_3$ , the  $\mu$  does not vanish as shown in Figure 3(a). It is to be noted that the magnitude of  $\mu$  is highest for  $CoCO_3$  in this series, which possesses the lowest  $T_N$ .

As we mentioned, the counter-intuitive  $H$  dependence of the *quasi-static* remanence has been observed for a number of DMI driven canted AFM [12–14, 16, 17]. Associated physical mechanism appears to be related to the interplay between the exchange, Zeeman and the magnetocrystalline anisotropy, with an additional factor associated with the spin-canting. This in turn relates to a specific domain pattern [14]. This domain pattern is likely to be different in canted-AFM as compared to a routine FM/AFM. The process of field cooling from above the  $T_N$  leads to imprinting of canted-AFM domains guided by the relative strength of various energy scales including exchange, Zeeman, magnetocrystalline anisotropy and DMI [14, 15]. Below a critical magnetic field, the canted-domains are formed by interplay between intrinsic DMI and Zeeman. Above a critical  $H$ , the Zeeman term dominates over DMI and the AFM domains are guided by the applied magnetic field rather than the DMI driven spin-canting. Thus, at very high magnetic field, the quasi static remanence vanishes. This seems to be related to unusual magnetic field dependence, which is reflected clearly in remanence, rather than *in-field* magnetization. These data indicate that at low fields the phenomenon of spin-canting is exclusively related to the *quasi static* part of the remanence.

It is to be noted that  $CoCO_3$  also shows a tendency to peak

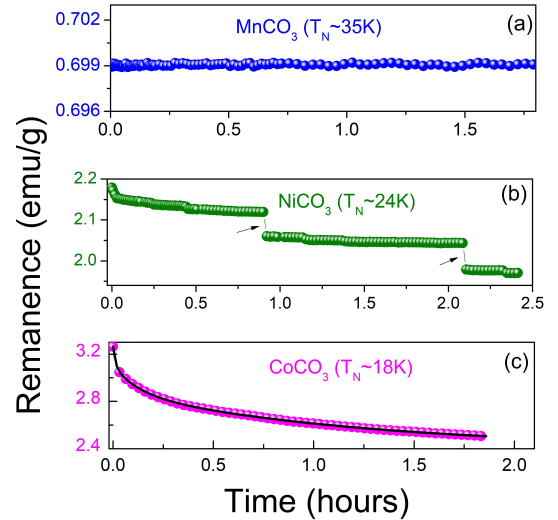


FIG. 4. (a)-(c) compares time-dependence of remanence at a fix temperature of 5K for all three carbonates. The remanent state in all three cases has been prepared at a fixed  $H=100$  Oe. The stability of *quasi-static* remanence is seen to be highest in  $MnCO_3$ , which has highest  $T_N$  in this series. The magnitude of the remanence is also lowest in this case. The remanence in case of  $NiCO_3$  exhibits avalanches like features, marked by arrows in (b). These features are exclusive to  $NiCO_3$  and reproducible when the remanent state is prepared in different magnetic fields.  $CoCO_3$ , with lowest  $T_N$  the  $\mu$  vs *time* follows the triple exponential decay, as shown with the black solid line in (c).

like behavior, but it does not eventually vanish with increasing  $H$ , unlike the other two carbonates (Figure 3a). Here we recall that the spin-canting in  $CoCO_3$  is known to have contributions from DMI as well as SIA.[10, 24–28]. The orbital magnetic moment in  $CoCO_3$  remains relatively more unquenched [11, 29] as compared to  $MnCO_3$  and  $NiCO_3$ . While DMI driven-spin canting relates to  $T_N$  through  $J$ , the exchange coupling constant, the SIA is understood to be independent of  $J$  and hence  $T_N$  [10]. With SIA also contributing to spin-canting (as is case of  $CoCO_3$ ) it appears that the process of field-cooling from above the  $T_N$  may lead the canted-domains to still remained pinned, when the remanent state is prepared in higher  $H$ . Whether  $\mu$  not vanishing with higher magnetic fields in  $CoCO_3$  indeed relates to SIA term being significant in  $CoCO_3$  needs further investigations. This can be confirmed by tracking the nature of remanence in pure SIA driven canted-AFM.

We note that the magnitude of this  $\mu$  is systematically largest in the sample with lowest  $T_N$ , which is  $CoCO_3$  in this series. Spin-canting angle is larger in samples with lower  $T_N$  [9, 10] which in-turn relates to the lower exchange coupling constant associated with the primary AFM phase. Thus DMI driven spin-canting angle is expected to be larger in samples with lower  $T_N$ . It is evident that this feature is clearly reflected in *quasi-static* remanence, rather than magnetization in this series as the magnitude of the *quasi-static* remanence is largest in the sample with lowest  $T_N$ . Overall, these data establish that all three samples exhibit a *quasi-static*  $\mu$  which is exclusively related to spin-canting phenomenon.

#### D. Remanence vs time in $\text{CoCO}_3$ , $\text{NiCO}_3$ and $\text{MnCO}_3$

The magnetization relaxation (i.e the time dependence of remanent magnetization) is an important tool for magnetic characterization. The remanent state in such measurements is also set by cooling (or heating) the sample through the transition temperature in various H, switching off the H and tracking the *time-dependence* of remanence. These measurements reveal the intricacies of magnetization dynamics in routine as well as complex magnetic systems [20, 30, 31]. We also measured magnetization relaxation phenomenon by tracking the time-dependence of  $\mu$  prepared in different (cooling) fields. We first prepare a particular remanent state by following the similar experimental protocol outlined in Figure 2(a). After the  $M_{FC}$  vs T run, the magnetic field is switched off at 5K and the variations of  $\mu$  with time ( $t$ ) is measured. The  $\mu$  vs  $t$  data clearly bring forward the *quasi-static* nature of remanence. For each sample, time dependence of  $\mu$  was recorded at several (cooling) magnetic fields. For the sake of comparison, the data obtained for the identical (cooling) field of 100 Oe has been plotted for all three carbonates. The magnetization relaxation in the time span of 1.5 to 2 hours for all three samples is compared in Figure 4. As is evident from Figure 4(a) the remanence exhibits hardly any decay with time in case of  $\text{MnCO}_3$ , the sample with  $T_N$  about 35K. Similar features are also seen in case of  $\text{NiCO}_3$ . However, the magnetization relaxation in the case of  $\text{NiCO}_3$  proceeds through several discrete jumps, each of which is *quasi-static* in nature, Figure 4(b). Several measurements were repeated in different (cooling) magnetic fields which confirm that these jumps are intrinsic to  $\text{NiCO}_3$ . We also emphasize that such jumps in *quasi-static* remanence were also observed in single-crystal hematite [12] as well as when hematite is encapsulated inside carbon nanotubes [14]. The observation of such jumps appears to indicate the depinning of domains which are exclusively related to canted phase. Thus, the existence of *quasi-static* remanence exclusively connects to the DMI driven canted AFM for both  $\text{MnCO}_3$  and  $\text{NiCO}_3$ . The stability of this *quasi-static* remanence relates to the Neel temperature and the critical magnetic field that is applied during the preparation of the remanent state.  $\text{CoCO}_3$  on the other hand exhibits a mixed contribution from *quasi-static*  $\mu$  along with some relatively faster time scales, Figure4(c). This is concluded from fitting the relaxation data to a triple exponential decay function, as shown in Figure 4(c).

$$\mu(t) = \mu_1 e^{-\frac{t}{\tau_1}} + \mu_2 e^{-\frac{t}{\tau_2}} + \mu_3 e^{-\frac{t}{\tau_3}}, \quad (1)$$

Here  $\tau_1$ ,  $\tau_2$  and  $\tau_3$  denote the three decay constants respectively. The solid line in the main panel represent the triple exponential fits to the  $\mu_{FC}$  versus time data. The decay times extracted for the particular H of 100 Oe yield  $\tau_1$  ( $= 0.01$  h)  $<$   $\tau_2$  ( $= 0.12$  h)  $<$   $\tau_3$  ( $= 1.22$  h). This implies that one of the time scale is ultra slow, with  $\tau$  in the scale of hours. While  $\text{CoCO}_3$  also exhibits ultra -slow magnetization relaxation that leads to the observation of  $\mu$ , the additional features as observed in this case appears to be related to the contribution of SIA and its strength as compared to other energy scales, including the

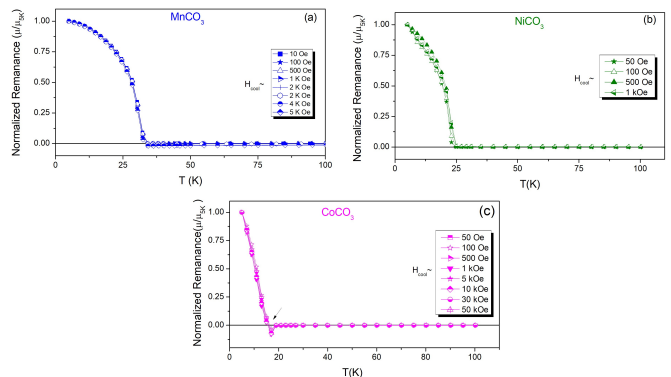


FIG. 5. (a) - (c) show normalized  $\mu$  vs T exhibiting scaling in remanence at selected H for all three carbonates and relate to the intrinsic phenomenon of piezomagnetism.

exchange and Zeeman. Again, relaxation data on pure SIA driven systems will be illuminating in this context .

Overall, we conclude that the stability of remanence with time reduces systematically for  $\text{MnCO}_3$ ,  $\text{NiCO}_3$  and  $\text{CoCO}_3$ , that possess progressively decreasing  $T_N$ . On the other hand, the magnitude of the *quasi-static* remanence remains highest for sample with lowest  $T_N$ , which is  $\text{CoCO}_3$ , but with a caveat that this sample also has contribution of SIA. Our core observation pertaining to magnitude of  $\mu$  is consistent with the fact that the spin-canting angle increases with decreasing J and hence it is larger for samples with lower  $T_N$ , especially for DMI driven systems. For SIA driven systems, spin-canting angle should not vary significantly with J and therefore with  $T_N$ . While primary mechanism of spin canting in  $\text{CoCO}_3$  is DMI, it is known to have contribution from SIA as well. Experimental and theoretical data has revealed that the spin canting angle is larger in  $\text{NiCO}_3$  as compared to  $\text{CoCO}_3$  [19]. The manifestation of SIA related factors appear to be reflected in the *time* as well as *magnetic-field* dependence of  $\mu$  of  $\text{CoCO}_3$ . Whether this dynamics captures the essential physics behind the canting mechanism (DMI, SIA or both) needs a comparative study on pure SIA-driven canted-AFM. From the present set of data, we expect *quasi-static* remanence to exist in spin-canted systems, but the *field* and *time* dependence of this *quasi-static* remanence may be different in DMI driven systems from the SIA driven ones. Exploring the functional form of  $\mu$  can thus provide insights in isolating the DMI or SIA contribution in new systems.

#### E. Scaling of *quasi-static* Remanence in $\text{CoCO}_3$ , $\text{NiCO}_3$ and $\text{MnCO}_3$

While the counter-intuitive magnetic field dependence along with *quasi-static* nature of remanence is observed in all three carbonates, which are symmetry allowed spin-canted systems, there is an associated phenomenon of piezomagnetism, which is equally intriguing[28, 32–34]. There have been reports from other groups that reveal a scaling phenomenon in remanence measurements in systems in which

piezomagnetism arises from size-effects or doping [15, 20]. This scaling is understood to arise from the observation that the remanence factorizes with temperature and magnetic field variables following the equation  $\mu_{FC}(H,T) = f(H)g(T)$ [15, 20]. This factorization leads to a universal scaling, when normalized remanences (prepared in different (cooling) magnetic fields) are plotted as a function of T. We have earlier observed this scaling phenomenon in a chrome -oxide based hybrid system in which the individual constituent is not a symmetry allowed piezomagnet, but arises due to interface effects [16]. In present case, all three carbonates are also symmetry allowed piezomagnets. In light of the fact that the remanence in  $\text{CoCO}_3$  is almost self-scaled, we were tempted to explore scaling effects in remaining two carbonates. These data are shown in Figure 5(a)-(c) for all three samples. Here  $\mu$  vs T runs, in which the magnitude of  $\mu$  that is not vanishingly small, are chosen. The rationale is that when  $\mu$  is negligibly small, the data are influenced by the residual magnetic field associated with the superconducting magnet of SQUID. This residual field is often negative and can lead to a residual (and negative) magnetization, as is highlighted with a black arrow in Figure 5(c) and also in Figure 2(d). This negative residual magnetization also becomes prominent in the vicinity of  $T_N$ , when  $\mu$  is about to vanish, as is evident from Figure 2(d) and Figure 5(c). Barring such runs, when we plot normalized  $\mu$  vs T at different (cooling) H, we do see a universal scaling in *quasi-static* remanence for all three samples. This observation is also consistent with previous reports on the scaling of *quasi-static* remanence in which the effect arises due to size and interface effects[16, 17]. This universal scaling as observed in all three carbonates confirms the concurrent phenomenon of piezomagnetism in spin-canted AFM .

### F. Neutron Diffraction in remanent state in $\text{CoCO}_3$

To gain microscopic evidence for the ultra-slow relaxation phenomena that leads to *quasi-static* remanence in these DMI driven systems, we performed neutron powder diffraction (NPD) measurements on a representative sample,  $\text{CoCO}_3$ . We have recorded the NPD patterns at two selected temperatures, 100 K and 1K. Considering that the  $T_N$  of  $\text{CoCO}_3$  is 18 K, the NPD recorded at 100 K covers the paramagnetic region and that recorded at 1K is in the AFM region. The data is recorded at these two fixed temperatures in (i) zero H (ii) in presence of  $H = 2\text{kOe}$  (iii) in the corresponding remanent state. These data are presented in Figure 6.

The sample is first cooled in zero magnetic field from the room temperature and NPD is recorded at 100 K (in the paramagnetic region for  $\text{CoCO}_3$ ). This is shown as open black circles in Figure 6(a). The peak indexing in Fig. 6(a) is consistent with the Plumier's work on neutron diffraction study on the isostructural compound  $\text{NiCO}_3$  [35, 36]. The indices in the NPD pattern are written with respect to R-3c space group in the hexagonal setting. The peaks marked with an asterisk arise from the cryomagnet during NPD measurements. It is worth mentioning here that there are no impurity peaks in XRD pattern of the  $\text{CoCO}_3$  sample (see supplemental infor-

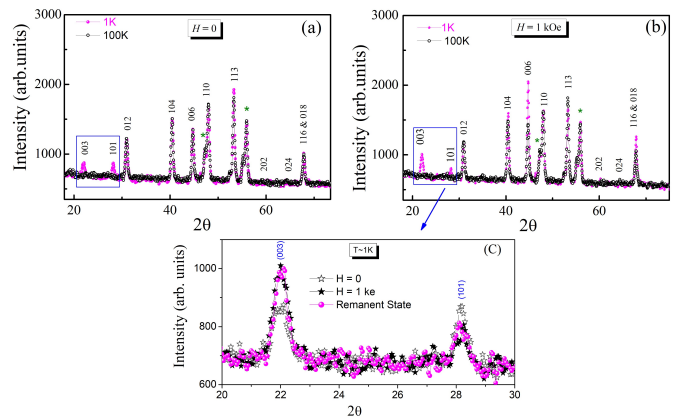


FIG. 6. (a) and (b) compares neutron powder diffraction data (NPD) at 100 K and 1K measured in zero magnetic field and in 1kOe respectively. The black dots in both cases represent NPD in paramagnetic region (100K) and pink dots show the same antiferromagnetic region (1K). The indices are written with respect to the R-3c space group in hex setting. The pure AFM peaks (003) & (110) are highlighted in (a) and (b). Data in (c) highlights NPD at 1K in zero H (open black stars) , 1kOe (filled black stars) and in corresponding remanent state (pink dots) for  $\text{CoCO}_3$  for pure AFM peaks.

mation, Text S3 for details).

After recording NPD at 100 K, the sample was further cooled to even lower temperatures in zero field and the NPD was recorded at 1K (below the  $T_N$  of  $\text{CoCO}_3$  ). These data are shown as pink- dots in Figure 6(a). It is evident from the comparison of the NPD profiles recorded at 1K and 100 K in Figure 6(a), the two additional peaks (003 and 101) other than the main perovskite peaks are present in the 1K NPD patterns. These purely magnetic peaks (003) and (101) at 1K are highlighted in Figure 6(a), as they are exclusive to AFM phase of  $\text{CoCO}_3$ . The additional magnetic Bragg peaks at 1K are indexed with a propagation vector  $k = (0,0,0)$  corresponding to the space group R-3c. The magnetic structures compatible with the R-3c symmetry are determined by representation analysis technique. For the propagation vector  $k = (0,0,0)$ , the magnetic reducible representation can be decomposed as direct sum of three irreducible representations, out of which only one explains the observed magnetic peaks and spin-canting model. For the sake of clarity, this detailed Rietveld profile refinement of the NPD data at each temperature and magnetic field is presented in supp. information Figure S3(a)-(d). The magnetic structure is also schematically shown in supp. Info, Figure S4.

For recording the *in-field* and the corresponding *remanent-state* NPD, the sample was again cooled from the room temperature down to 100 K in the presence of 1 kOe magnetic field. The NPD was recorded at  $T = 100\text{K}$  in the paramagnetic region of  $\text{CoCO}_3$  , in presence of 1kOe. These data are shown as black circles in Figure 6(b). The sample was then cooled down to to 1K and the NPD was recorded in presence of 1 kOe magnetic field. This patterns is shown as pink dots in Figure 6(b). We note from the Figure 6(b) that in the presence of magnetic field, the intensity of the strongest magnetic peak

(003) increases significantly, as compared to the zero-field NPD pattern. Subsequently, the magnetic field is switched-off and NPD is now recorded in remanent state, while temperature is still held at 1K. It is to be noted that the entire protocol of measuring this remanent state NPD is similar to what is adopted to track remanence using SQUID magnetometry.

We finally compare NPD pattern at 1K in zero magnetic field, in presence of 1kOe magnetic field and in the corresponding remanent state in Figure 6(c). Here, for the sake of clarity we focus on (003) and (101) peaks, which are pure AFM peaks. Figure 6(c) clearly shows that the intensity of the strongest peak (003) in the presence of magnetic field and in the remanent state are comparable. This suggests that the NPD data not only show the relative change in intensity in the presence of H, but also confirms that the intensity is retained in the remanent state. Microscopically, these data demonstrate that once the canted domains have been guided during the field cooling process, their rearrangement is energetically unfavorable after the magnetic field is removed. This feature in NPD relates to the *quasi-static* remanence, which we observe in bulk magnetization through SQUID magnetometry. The NPD data further confirm the ultra-slow magnetization dynamics associated with canted AFM, which is also reflected in the bulk magnetometry. Thus, in addition to our bulk magnetization measurements, NPD data further supports the presence of *quasi-static* remanence and its connection with spin-canting.

### III. CONCLUSIONS

In conclusion, we have conducted remanence measurements in a series of carbonates which are prototypical canted-antiferromagnets and piezomagnets with systematically varying  $T_N$ . These are primarily Dzyaloshinskii Moriya Interaction driven systems. However, contribution of single ion anisotropy is significant for  $\text{CoCO}_3$ , as compared to other two carbonates.

All three samples exhibit a unique feature in remanence, a part which is *quasi-static* in nature and exhibits a counter-intuitive magnetic field dependence. The magnitude of this *quasi-static* remanence shows a systematic variation with  $T_N$  and therefore with the extent of spin-canting. The magnitude is larger for sample with smaller  $T_N$ , which is  $\text{CoCO}_3$  in this series of compounds. The stability of remanence with respect to time is higher for samples with higher  $T_N$ , which is  $\text{MnCO}_3$ .  $\text{NiCO}_3$  shows a similar feature, albeit with discrete jumps. The normalized remanence also exhibits a universal scaling for all three samples, which appears to be associated with the concurrent phenomenon of piezomagnetism. The existence of this *quasi-static* remanence is also seen in neutron diffraction, conducted in remanent state. The specifics related to the variation of *quasi-static* remanence with *magnetic field* or *time* can provide crucial information for isolating the Dzyaloshinskii Moriya Interaction driven canted-antiferromagnets from single-ion-anisotropy driven ones.

### SUPPLEMENTARY MATERIAL

See the Supplementary Information for synthesis details of Mn, Ni and  $\text{CoCO}_3$  in Text S1 & Text S2. X-Ray diffraction patterns along with the Rietveld Profile refinement of XRD data and low field MH for all three carbonates is given as Figure S1 and Figure S2 respectively. Neutron diffraction data along with Rietveld profile refinements and magnetic structure details of sample  $\text{CoCO}_3$  in section III of SI.

### ACKNOWLEDGEMENTS

SN thanks the Department of Science and Technology, India (SR/NM/Z-07/2015) for financial support to carry out the neutron diffraction experiment, and Jawaharlal Nehru Centre for Advanced Scientific Research (JNCASR) for managing the project. AB acknowledges DST-SERB grant, India (CRG/2022/008373) for funding support.

- 
- [1] B. Binz, A. Vishwanath, and V. Aji, Theory of the helical spin crystal: A candidate for the partially ordered state of mnsi, Phys. Rev. Lett. **96**, 207202 (2006).
- [2] J. Gayles, F. Freimuth, T. Schena, G. Lani, P. Mavropoulos, R. A. Duine, S. Blügel, J. Sinova, and Y. Mokrousov, Dzyaloshinskii-moriya interaction and hall effects in the skyrmion phase of  $\text{mn}_{1-x}\text{fe}_x\text{Ge}$ , Phys. Rev. Lett. **115**, 036602 (2015).
- [3] J. Sinova and I. Zutic, Nature Materials **11**, 368 (2012).
- [4] V. Baltz, A. Manchon, M. Tsoi, T. Moriyama, T. Ono, and Y. Tserkovnyak, Antiferromagnetic spintronics, Rev. Mod. Phys. **90**, 015005 (2018).
- [5] F. Ajejas, A. Gudín, R. Guerrero, A. Anadón Barcelona, J. M. Diez, L. de Melo Costa, P. Olleros, M. A. Niño, S. Pizzini, J. Vogel, *et al.*, Unraveling dzyaloshinskii–moriya interaction and chiral nature of graphene/cobalt interface, Nano letters **18**, 5364 (2018).
- [6] K. Di, V. L. Zhang, H. S. Lim, S. C. Ng, M. H. Kuok, J. Yu, J. Yoon, X. Qiu, and H. Yang, Direct observation of the dzyaloshinskii-moriya interaction in a pt/co/ni film, Phys. Rev. Lett. **114**, 047201 (2015).
- [7] P. Němec, M. Fiebig, T. Kampfrath, and A. V. Kimel, Antiferromagnetic opto-spintronics, Nature Physics **14**, 229 (2018).
- [8] C. Weingart, N. Spaldin, and E. Bousquet, Noncollinear magnetism and single-ion anisotropy in multiferroic perovskites, Phys. Rev. B **86**, 094413 (2012).
- [9] I. E. Dzyaloshinskii, JETP **32**, 1259 (1957).
- [10] T. Moriya, Phys. Rev. **120**, 91 (1960).
- [11] D. Pincini, F. Fabrizi, G. Beutier, G. Nisbet, H. Elnaggar, V. E. Dmitrienko, M. I. Katsnelson, Y. O. Kvashnin, A. I. Liechtenstein, V. V. Mazurenko, E. N. Ovchinnikova, O. V. Dimitrova, and S. P. Collins, Role of the orbital moment in a series of isostructural weak ferromagnets, Phys. Rev. B **98**, 104424 (2018).
- [12] N. Pattanayak, A. Bhattacharyya, A. K. Nigam, S.-W. Cheong, and A. Bajpai, Quasistatic remanence in dzyaloshinskii-moriya interaction driven weak ferromagnets and piezomagnets, Phys. Rev. B **96**, 104422 (2017).

- [13] N. Pattanayak, A. Bhattacharyya, S. Chakravarty, and A. Bajpai, Weak ferromagnetism and time-stable remanence in hematite: effect of shape, size and morphology, *Journal of Physics: Condensed Matter* **31**, 365802 (2019).
- [14] A. Kapoor, A. B. Dey, C. Garg, and A. Bajpai, Enhanced magnetism and time-stable remanence at the interface of hematite and carbon nanotubes, *Nanotechnology* **30**, 385706 (2019).
- [15] S. Sahoo and C. Binek, Piezomagnetism in epitaxial  $\text{Cr}_2\text{O}_3$  thin films and spintronic applications, *Philosophical Magazine Letters* **87**, 259 (2007).
- [16] A. Bajpai, R. Klingeler, N. Wizen, A. K. Nigam, S.-W. Cheong, and B. Büchner, Unusual field dependence of remanent magnetization in granular  $\text{CrO}_2$ : the possible relevance of piezomagnetism, *Journal of Physics: Condensed Matter* **22**, 096005 (2010).
- [17] A. Bajpai, Z. Aslam, S. Hampel, R. Klingeler, and N. Grobert, A carbon-nanotube based nano-furnace for in-situ restructuring of a magnetoelectric oxide, *Carbon* **114**, 291 (2017).
- [18] I. Gross, L. J. Martínez, J.-P. Tetienne, T. Hingant, J.-F. Roch, K. Garcia, R. Soucaille, J. P. Adam, J.-V. Kim, S. Rohart, A. Thiaville, J. Torrejon, M. Hayashi, and V. Jacques, Direct measurement of interfacial dzyaloshinskii-moriya interaction in  $x|\text{CoFeB}|/\text{MgO}$  heterostructures with a scanning nv magnetometer ( $x = \text{Ta}, \text{TaN}, \text{and W}$ ), *Phys. Rev. B* **94**, 064413 (2016).
- [19] G. Beutier, S. P. Collins, O. V. Dimitrova, V. E. Dmitrienko, M. I. Katsnelson, Y. O. Kvashnin, A. I. Lichtenstein, V. V. Mazurenko, A. G. A. Nisbet, E. N. Ovchinnikova, and D. Pincini, Band filling control of the dzyaloshinskii-moriya interaction in weakly ferromagnetic insulators, *Phys. Rev. Lett.* **119**, 167201 (2017).
- [20] J. Kushauer, W. Kleemann, J. Mattsson, and P. Nordblad, Crossover from logarithmically relaxing to piezomagnetically frozen magnetic remanence in low-field-cooled  $\text{Fe}_{0.47}\text{Zn}_{0.53}\text{F}_2$ , *Phys. Rev. B* **49**, 6346 (1994).
- [21] K. Binder and A. P. Young, Spin glasses: Experimental facts, theoretical concepts, and open questions, *Rev. Mod. Phys.* **58**, 801 (1986).
- [22] N. Kreines and T. Shal'Nikova, Weak ferromagnetism in  $\text{NiCO}_3$ , *Soviet Physics JETP* **31** (1970).
- [23] V. C. Srivastava, Effect of pressure on the néel temperature of  $\text{MnCO}_3$ ,  $\text{CoCO}_3$ , and  $\text{FeCO}_3$ , *Journal of Applied Physics* **41**, 1190 (1970).
- [24] A. H. Morrish, *Canted Antiferromagnetism: Hematite* (WORLD SCIENTIFIC, 1995).
- [25] P. Radhakrishna, Polarized neutron diffraction studies on weak ferromagnetism—a survey, *Le Journal de Physique Colloques* **43**, C7 (1982).
- [26] S. N. Martynov, Single-ion mechanism of weak ferromagnetism and a spin-flop transition in one- and two-position antiferromagnets, *JETP Letters* **108**, 196 (2018).
- [27] A. Borovik-Romanov, A. Bazhan, and N. Kreines, The weak ferromagnetism of  $\text{NiF}_2$ , *Soviet Journal of Experimental and Theoretical Physics* **37**, 695 (1973).
- [28] A. B. Romanov, *Soviet Physics JETP* **11**, 786 (1960).
- [29] V. Loktev, Spin excitations of  $\text{CoCO}_3$  in a longitudinal magnetic field, *Physics Letters A* **81**, 187 (1981).
- [30] M. J. Benitez, O. Petravic, E. L. Salabas, F. Radu, H. Tüysüz, F. Schüth, and H. Zabel, Evidence for core-shell magnetic behavior in antiferromagnetic  $\text{Co}_3\text{O}_4$  nanowires, *Phys. Rev. Lett.* **101**, 097206 (2008).
- [31] M. J. Benitez, O. Petravic, H. Tüysüz, F. Schüth, and H. Zabel, Fingerprinting the magnetic behavior of antiferromagnetic nanostructures using remanent magnetization curves, *Phys. Rev. B* **83**, 134424 (2011).
- [32] I. E. Dzyaloshinskii, *JETP* **33**, 807 (1957).
- [33] L. D. Landau and E. Lifshitz, *Electrodynamics of Continuous Media* (Pergamon Press Ltd., 1984).
- [34] S. A. J. Kimber and J. P. Attfield, Magnetic order in acentric  $\text{Pb}_2\text{MnO}_4$ , *J. Mater. Chem.* **17**, 4885 (2007).
- [35] R. Plumier, M. Sougi, M. Lecomte, and R. Saint-James, Weak ferromagnetism in  $\text{NiCO}_3$ , *Journal of Applied Physics* **57**, 3261 (1985).
- [36] R. Plumier, M. Sougi, and R. Saint-James, Neutron-diffraction reinvestigation of  $\text{NiCO}_3$ , *Phys. Rev. B* **28**, 4016 (1983).
- [37] T. T. Smith, The magnetic properties of hematite, *Physical Review* **8**, 721 (1916).
- [38] A. McDannald, L. Kuna, M. S. Seehra, and M. Jain, Magnetic exchange interactions of rare-earth-substituted  $\text{dycro}_3$  bulk powders, *Phys. Rev. B* **91**, 224415 (2015).
- [39] D. I. Khomskii, *Transition metal compounds* (Cambridge University Press, 2014).
- [40] F. Morin, Magnetic susceptibility of  $\alpha\text{-Fe}_2\text{O}_3$  and  $\alpha\text{-Fe}_2\text{O}_3$  with added titanium, *Physical Review* **78**, 819 (1950).
- [41] Y. Onose, T. Ideue, H. Katsura, Y. Shiomi, N. Nagaosa, and Y. Tokura, Observation of the magnon hall effect, *Science* **329**, 297 (2010).
- [42] M. Z. Hasan and C. L. Kane, Colloquium, *Rev. Mod. Phys.* **82**, 3045 (2010).
- [43] O. Gomonay, V. Baltz, A. Brataas, and Y. Tserkovnyak, *Nature Physics* **14**, 213 (2018).
- [44] A. S. Borovik-Romanov, *Zh. Eksp. Teor. Fiz.* **38**, 1088 (1960).
- [45] V. Andratskii and A. S. Borovik-Romanov, *JETP* **687**, 1036 (1966).
- [46] A. S. Borovik-Romanov, *Ferroelectrics* **162**, 153 (1994).
- [47] S. A. J. Kimber and J. P. Attfield, Magnetic order in acentric  $\text{Pb}_2\text{MnO}_4$ , *J. Mater. Chem.* **17**, 4885 (2007).
- [48] T. G. Phillips, R. L. Townsend, and R. L. White, Piezomagnetism of  $\text{CoF}_2$  and  $\alpha\text{-Fe}_2\text{O}_3$  from electron-paramagnetic-resonance pressure experiments, *Phys. Rev. Lett.* **18**, 646 (1967).
- [49] T. G. Phillips, R. L. Townsend, and R. L. White, Piezomagnetism of  $\alpha\text{-Fe}_2\text{O}_3$  and the magnetoelastic tensor of  $\text{Fe}^{3+}$  in  $\text{Al}_2\text{O}_3$ , *Phys. Rev.* **162**, 382 (1967).
- [50] Binek, Ch., Borisov, P., Chen, Xi, Hochstrat, A., Sahoo, S., and Kleemann, W., Perpendicular exchange bias and its control by magnetic, stress and electric fields, *Eur. Phys. J. B* **45**, 197 (2005).
- [51] O. Özdemir and D. J. Dunlop, *Geochem. Geophys. Geosyst.* **9**, 1 (2008).
- [52] N. Amin and S. Arajs, Morin temperature of annealed submicronic  $\alpha\text{-Fe}_2\text{O}_3$  particles, *Phys. Rev. B* **35**, 4810 (1987).
- [53] R. D. Zysler, D. Fiorani, A. M. Testa, L. Suber, E. Agostinelli, and M. Godinho, Size dependence of the spin-flop transition in hematite nanoparticles, *Phys. Rev. B* **68**, 212408 (2003).
- [54] S. Mitra, S. Das, S. Basu, P. Sahu, and K. Mandal, Shape- and field-dependent morin transitions in structured  $\alpha\text{-Fe}_2\text{O}_3$ , *Journal of Magnetism and Magnetic Materials* **321**, 2925 (2009).
- [55] S. Mørup and C. Frandsen, Thermoinduced magnetization in nanoparticles of antiferromagnetic materials, *Phys. Rev. Lett.* **92**, 217201 (2004).
- [56] M. J. Benitez, O. Petravic, H. Tüysüz, F. Schüth, and H. Zabel, Fingerprinting the magnetic behavior of antiferromagnetic nanostructures using remanent magnetization curves, *Phys. Rev. B* **83**, 134424 (2011).
- [57] M. J. Benitez, O. Petravic, E. L. Salabas, F. Radu, H. Tüysüz, F. Schüth, and H. Zabel, Evidence for core-shell magnetic behavior in antiferromagnetic  $\text{Co}_3\text{O}_4$  nanowires, *Phys. Rev. Lett.* **101**, 097206 (2008).



- [58] J. Mattsson, C. Djurberg, and P. Nordblad, Low-temperature magnetization in dilute ising antiferromagnets, *Phys. Rev. B* **61**, 11274 (2000).
- [59] M. Suzuki, I. S. Suzuki, and M. Matsuura, Memory and aging effect in hierarchical spin orderings of the stage-2  $\text{CoCl}_2$  graphite intercalation compound, *Phys. Rev. B* **73**, 184414 (2006).
- [60] L. Chen, X. Yang, J. Chen, J. Liu, H. Wu, H. Zhan, C. Liang, and M. Wu, Continuous shape- and spectroscopy-tuning of hematite nanocrystals, *Inorganic Chemistry* **49**, 8411 (2010).
- [61] X. Liu, J. Zhang, S. Wu, D. Yang, P. Liu, H. Zhang, S. Wang, X. Yao, G. Zhu, and H. Zhao, Single crystal  $\alpha\text{-Fe}_2\text{O}_3$  with exposed 104 facets for high performance gas sensor applications, *RSC Adv.* **2**, 6178 (2012).
- [62] R. Young, *The Rietveld Method* (International Union of Crystallography, Oxford University Press, 1995).
- [63] A. H. Hill, F. Jiao, P. G. Bruce, A. Harrison, W. Kockelmann, and C. Ritter, Neutron diffraction study of mesoporous and bulk hematite,  $\alpha\text{-Fe}_2\text{O}_3$ , *Chemistry of Materials* **20**, 4891 (2008).
- [64] P. A. Joy, P. S. A. Kumar, and S. K. Date, The relationship between field-cooled and zero-field-cooled susceptibilities of some ordered magnetic systems, *Journal of Physics: Condensed Matter* **10**, 11049 (1998).
- [65] S. Blundell, *Magnetism in Condensed Matter*, (Oxford University Press, 2001).
- [66] J. Sandonis, J. Baruchel, B. Tanner, G. Fillion, V. Kvardakov, and K. Podurets, *Journal of Magnetism and Magnetic Materials* **104**, 350 (1992).
- [67] R. Yanes, J. Jackson, L. Udvardi, L. Szunyogh, and U. Nowak, Exchange bias driven by dzyaloshinskii-moriya interactions, *Phys. Rev. Lett.* **111**, 217202 (2013).
- [68] S. Bae, J. H. Judy, P. J. Chen, and W. F. Egelhoff, Dependence of physical properties and giant magnetoresistance ratio on substrate position during rf sputtering of nio and  $\alpha\text{-Fe}_2\text{O}_3$  for bottom spin valves, *Applied Physics Letters* **81**, 2208 (2002).
- [69] Y. Kawawake, Y. Sugita, M. Satomi, and H. Sakakima, Spin valves with a thin pinning layer of  $\alpha\text{-Fe}_2\text{O}_3$  or  $\alpha\text{-Fe}_2\text{O}_3/\text{nio}$ , *Journal of Applied Physics* **85**, 5024 (1999).
- [70] G. Rollmann, A. Rohrbach, P. Entel, and J. Hafner, First-principles calculation of the structure and magnetic phases of hematite, *Phys. Rev. B* **69**, 165107 (2004).
- [71] R. R. Birss, *Symmetry and Magnetism* (New York: North-Holland Pub. Co., 1964).